HHS Public Access

Author manuscript

Leuk Lymphoma. Author manuscript; available in PMC 2021 February 01.

Published in final edited form as:

Leuk Lymphoma. 2020 February ; 61(2): 409–419. doi:10.1080/10428194.2019.1672055.

Parathyroid hormone-related protein promotes bone loss in T-cell leukemia as well as in solid tumors

Nicole A. Kohart[1], **Said M. Elshafae**[1,4], **Aylin A. Demirer**[1,5], **Wessel P. Dirksen**[1], **Justin T. Breitbach**[1], **Sherry T. Shu**[6], **Jingyu Xiang**[2], **Katherine N. Weilbaecher**[2], **Thomas J. Rosol**[1,3,*]

[1]Department of Veterinary Biosciences, College of Veterinary Medicine, The Ohio State University, Columbus, OH 43210, USA

[2]Department of Medicine, Division of Oncology, Washington University School of Medicine, St. Louis, MO 63110, USA

[3]Department of Biomedical Sciences, Heritage College of Osteopathic Medicine, Ohio University, Athens, OH 45701, USA

[4]Department of Pathology, Faculty of Veterinary Medicine, Benha University, Kalyubia, Postal Code: 13736, Egypt

[5]Department of Pathology, Faculty of Veterinary Medicine, Bursa Uludag University, 16059 Bursa, Turkey

[6]Department of Microbiology and Molecular Genetics, School of Medicine, University of Pittsburgh, Pittsburgh, PA 15219, USA

Abstract

Parathyroid hormone-related protein (PTHrP) and macrophage inflammatory protein-1α (MIP-1α) are important factors that increase bone resorption and hypercalcemia in Adult T-cell Leukemia (ATL). We investigated the role of PTHrP and MIP-1α in the development of local osteolytic lesions in T-cell leukemia through overexpression in Jurkat T-cells. Injections of Jurkat-PTHrP and Jurkat-MIP-1α into the tibia and the left ventricle of NSG mice were performed to evaluate tumor growth and metastasis *in vivo*. Jurkat-pcDNA tibial neoplasms grew at a significantly greater rate and total tibial tumor burden was significantly greater than Jurkat-PTHrP neoplasms. Despite the lower tibial tumor burden, Jurkat-PTHrP bone neoplasms had significantly greater osteolysis than Jurkat-pcDNA and Jurkat-MIP-1α neoplasms. Jurkat-PTHrP and Jurkat-pcDNA cells preferentially metastasized to bone following intracardiac injection, though the overall metastatic burden was lower in Jurkat-PTHrP mice. These findings demonstrate that PTHrP induced pathologic osteolysis in T-cell leukemia but did not increase the incidence of skeletal metastasis.

Keywords

Cell Lines and Animal Models; T-cell Leukemia; PTHrP; MIP-1α; Metastasis; Bone resorption

[*]Corresponding author: Thomas Rosol, DVM, PhD, HCOM, Biomedical Sciences, 225 Irvine Hall, Athens, OH 45701, 740-593-2405, rosolt@ohio.edu.

Introduction

Adult T cell leukemia/lymphoma (ATL) is an aggressive liquid malignancy of CD4+ T-lymphocytes that occurs in 2–5% of human T-cell leukemia virus type-1 (HTLV-1)–infected individuals [1,2]. Studies have shown that ATL cells constitutively express genes known to promote pathologic osteoclast differentiation and activation, such as PTHrP and MIP-1α [3]. HTLV-1 also encodes two viral oncogenes, Tax and HBZ that have both been shown to upregulate the expression of bone signaling genes. The mechanisms on how these factors and transformed ATL cells modulate the bone microenvironment remain incompletely understood.

Parathyroid hormone-related protein (PTHrP) is frequently increased in the serum of patients with advanced ATL and is an important mediator of cancer-associated hypercalcemia and bone lesions observed in these patients [4–10]. PTHrP also mediates its actions on local tumor and stromal cells through paracrine, autocrine, and intracrine mechanisms when cancers metastasize to bone [11–14]. In bone metastatic cancers, PTHrP promotes metastasis through tumor cell-autonomous means and modification of the tumor microenvironment [13]. PTHrP may act in an intracrine manner to increase cell survival and prevent apoptosis, while also playing a role in modulating the bone microenvironment through signaling to resident bone cells [15]. PTHrP has also been described to have additional roles in the bone metastatic cascade. The emerging notion that endocrine-acting PTHrP from the primary tumor can modify the distant bone pre-metastatic niche to promote bone metastasis has been proposed in other bone-tropic neoplasms and may play a role in early ATL metastasis [13]. While the regulation of PTHrP in ATL and the endocrine role it plays in mediating HHM have been extensively studied, the paracrine effect of PTHrP on the bone microenvironment in ATL bone metastasis remains largely unknown.

Several reports have shown that primary ATL bone tumors express osteoclast-activating factors other than PTHrP [16,17]. MIP-1α has been frequently identified and implicated as a key factor in ATL-associated hypercalcemia and osteolytic bone lesions [16,18,19]. MIP-1α promotes ATL invasion and metastasis by inducing integrin-mediated adhesion of ATL cells and extravasation into distant tissues [20]. Recruitment and differentiation of osteoclasts are important roles of MIP-1α in promoting pathologic osteolysis [21,22]. MIP-1α has been shown to stimulate osteoclast activation through RANKL-dependent and independent mechanisms in multiple myeloma [23].

When ATL and HTLV-1-infected cells are introduced into the tibia of mice, several different pathologic bone changes are observed. Phenotypes resulting from tumor-bone interactions range from marked pathologic osteolysis to pathologic intramedullary new bone formation (sclerosis) (Kohart et al., JBO, in press). Tumor-bearing tibias demonstrating the greatest degree of osteolysis and osteoclast activity had the highest levels of PTHrP and MIP-1α mRNA when compared to those with either little to no bone response or an osteoblastic phenotype. These data suggested that PTHrP and MIP-1α act on the bone microenvironment to promote pathologic osteolysis via a paracrine mechanism in primary ATL bone neoplasms.

In this study, we hypothesized that T-lymphocyte expression of PTHrP or MIP-1α alone was sufficient to induce the pathologic osteolysis observed in ATL bone tumors via a paracrine mechanism.

Materials and Methods

Cell Lines

Human T cell leukemia Jurkat cell line with stable transfection of PTHrP, MIP-1α, or pcDNA3.1 vector and luciferase expression were previously generated and characterized [24]. These three cell lines Jurkat-pcDNA-luc, Jurkat-PTHrP-luc, and Jurkat-MIP-1α-luc will be referred to as Jurkat-pcDNA, Jurkat-PTHrP, or Jurkat-MIP-1α throughout this paper. Real-time RT-PCR (qRT-PCR) was used to confirm expression levels of PTHrP and MIP-1α mRNA for this study (not shown; see ref. [24] for original figure). Secretion of PTHrP in Jurkat-PTHrP cells was confirmed by immunoassay at the Diagnostic Center for Population and Animal Health at Michigan State University {Jurkat-PTHrP (42.4 pmol/l)}. The cells were cultured in RPMI 1640 medium supplemented with 10% FBS, 2 mM glutamine, and antibiotics (50 μg/ml streptomycin and 50 U/ml penicillin) at 37°C and 5% CO_2.

Mouse injections and bioluminescent imaging

All animal experiments were approved by The Ohio State University Institutional Laboratory Animal Care and Use Committee. Mice were purchased from the Target Validation Shared Resource (The Ohio State University, Columbus, OH).

Intratibial injections

Five, 4–6-week-old male NSG mice per group were injected into the marrow cavity of their tibias with 10 μL of RPMI medium containing a suspension of 250,000 Jurkat-pcDNA, Jurkat-PTHrP, or Jurkat-MIP-1α cells, as previously described [25].

Intracardiac injections

Five NSG male mice per group were injected into the left ventricle with 0.1 mL of RPMI medium containing a suspension of 1 million Jurkat-pcDNA or Jurkat-PTHrP cells, as previously described [25].

Bioluminescent imaging

Bioluminescent imaging was performed weekly, as previous described [25].

Measurement of plasma calcium concentrations

Mice were euthanized at the end of the study and blood was collected and placed into lithium heparin blood collection tubes. After mixing, tubes were centrifuged to separate the plasma. Total calcium concentrations were measured from the plasma of each mouse using the QuantiChrom Calcium Assay Kit (BioAssay Systems, Hayward, CA, USA).

Radiography

Radiographs of the tibias of mice with intratibial and intracardiac injections were performed postmortem. Tibias were fixed in 10% neutral-buffered formalin for 48 hours and then placed in 70% ethanol for 72 hours. Tibias were placed centrally on a Faxitron laboratory radiography system LX-60 (Faxitron X-ray Corp., Wheeling, IL) imaging platform and high-resolution radiographs were taken at 29 kV with 7 second exposures. The degree of radiolucency was used as a surrogate for bone loss and was quantified using Bioquant Osteo 2010 (Version 10.3.60MR). Radiograph dicom images were uploaded, the perimeter of each tibia was outlined and areas of radiolucency were then outlined and measured for each tibia. Percent of tumor-associated bone loss was calculated by dividing the area of radiolucency (bone loss) over the total tibial area for each sample.

Histopathology, Immunohistochemistry, Histomorphometry

Complete necropsies were performed on all mice. Following Faxitron imaging, tibias were decalcified in 10% EDTA (pH 7.4) for two weeks at 4°C and embedded in paraffin. Tibias from mice with intratibial injections were stained for tartrate-resistant acid phosphatase (TRAP) (Sigma-Aldrich (kit #387A), St. Louis, MO). PTHrP immunohistochemistry was performed on Jurkat-PTHrP and Jurkat-pcDNA bone tumors using rabbit polyclonal anti-PTHrP/PTH antibody (Santa Cruz (#sc-9860), Dallas, TX). Tissue from equine pituitary gland was used as a positive control. H&E and TRAP-stained slides were scanned at 20x using a Nanozoomer scanner (Hamamatsu Nanozoomer, Washington University, St. Louis, MO) and trabecular bone perimeter, osteoclast number, and osteoclast perimeter were measured using Bioquant software (Bioquant Osteo 2013 Version 13.2.60). To calculate trabecular volume per (total) bone volume (TV/BV), total tibial area from just below the growth plate to the proximal-mid diaphysis was outlined and measured for each H&E-stained tibia. Trabecular bone was then outlined and measured. The area of trabecular bone was divided by total tibial area to calculate the TV/BV. Trabecular bone perimeter from TRAP-stained tibias of each mouse was outlined and measured, and each osteoclast that was lining trabecular bone (identified by a TRAP-positive, burgundy-red color) was quantified. The number of osteoclasts was then divided by the surface (mm) of trabecular bone perimeter.

Calvarial bone culture

Conditioned media was collected from Jurkat-PTHrP, Jurkat-MIP-1α, and Jurkat-pcDNA cell lines. Forty-million cells of each cell type were cultured in T-75 flasks containing 20 mL of serum-free RPMI 1640 media supplemented with L-glutamine and penicillin/streptomycin for 48 hours in 37°C and 5% CO_2. After 48 hours, cells were centrifuged and the media was collected and stored at −80°C until use.

Calvarial disks were harvested as previously described [3] from 4–6-day-old heterozygous, nude mouse pups obtained from the Target Validation Shared Resource Center (The Ohio State University, Columbus, OH). Paired disks were randomly assigned to culture in 50% bone culture medium and 50% of the 48-hour conditioned media from Jurkat-pcDNA cells (n=20) for one disk and either Jurkat-PTHrP (n=10) or Jurkat-MIP-1α (n=10) conditioned media for the other disk in any given pair. On the sixth day of co-culture, medium was

harvested and total calcium concentrations were measured using the QuantiChrom Calcium Assay Kit (BioAssay Systems, Hayward, CA, USA). Calvarial bone disks were fixed and stained for TRAP activity using the TRAP staining kit (Sigma-Aldrich (kit #287A, St. Louis, MO).

Statistical Analysis

Data was analyzed using Graph Pad Prism 6.0 software (San Diego, CA). Students *t*-test and analysis of variance (ANOVA) tests were used for statistical analysis. A p value ≤ 0.05 was considered to be statistically significant. For the *in vivo* study, the average bioluminescence (photons/sec/cm^2) and corresponding standard deviations were determined for each experiment. Bioluminescence from the three groups of mice were compared using a one-way ANOVA. Calvarial surface area and calcium concentrations in the conditioned media of calvaria co-cultures were analyzed using a one-way ANOVA. Continuous variables including plasma calcium concentrations, and histomorphometry values, osteoclast number and trabecular bone perimeter were analyzed using a one-way ANOVA.

Results

PTHrP from Jurkat-PTHrP cells stimulated *ex vivo* bone resorption

PTHrP and MIP-1α are two factors that have demonstrated a significant role in endocrine-mediated bone resorption and HHM but the paracrine role of these factors in ATL remains unknown. To investigate the individual contributions of PTHrP and MIP-1α on local osteolysis, we made use of cell lines that we had previously generated and used for an intraperitoneal injection study [24].

To model the effect of secreted factors from tumor cells on bone *ex vivo*, calvarial discs from neonatal mice were co-cultured in 48-hour conditioned media from Jurkat-PTHrP, Jurkat-MIP-1α, or Jurkat-pcDNA cells. Calvarial discs were TRAP-stained to evaluate the distribution and extent of osteoclast activity (Figure 1A–D). Activated osteoclasts resorb the bone matrix and subsequently release growth factors and calcium stored in the mineralized matrix. Thus, calcium concentrations were measured in the medium to assess bone resorption. Calcium concentrations were greater in the medium of calvarial discs co-cultured with conditioned medium from Jurkat-PTHrP cells compared to the Jurkat-MIP-1α and Jurkat-pcDNA cells (Figure 1F). The increase in calcium paralleled the decrease in relative surface area in the corresponding calvarial disc. The area of each disc was measured using Bioquant Imaging software. There was a significant decrease in calvarial area in the discs co-cultured with the Jurkat-PTHrP conditioned media compared to the Jurkat-MIP-1α and Jurkat-pcDNA discs (Figure 1E). This experiment demonstrated that the effects of Jurkat-PTHrP cells on bone are due to the secretion of PTHrP acting locally on bone as the primary mechanism of bone resorption from these cells.

PTHrP and MIP-1α decreased intratibial tumor growth in Jurkat cells

To investigate the individual contributions of PTHrP and MIP-1α on local osteolysis in T-cell leukemia bone metastases, we injected the Jurkat cell lines into the tibias of immunosuppressed NSG mice. *In vivo* bioluminescent imaging of the injected mice was

performed weekly. By day 8, signal was observed in the tibias of all mice in the Jurkat-PTHrP group (Figure 2A). The relative bioluminescent signal was similar among all mice on the day of injection. On day 30 (day of sacrifice), tumor bioluminescence increased in all groups, and evidence of metastasis was observed in the lung and liver (Figure 2). Jurkat-PTHrP tibial neoplasms grew at a significantly slower rate compared to Jurkat-pcDNA tumors (Figure 2). On the day of sacrifice, tumor bioluminescence was significantly lower in Jurkat-PTHrP tibial neoplasms compared to Jurkat-pcDNA neoplasms (Figure 2). Jurkat-MIP-1α tibial neoplasms also grew slower and tumor burden was lower on the day of sacrifice compared to Jurkat-pcDNA, but the difference was not statistically significant.

Overexpression of PTHrP alone was sufficient to induce pathologic osteolysis in Jurkat intratibial bone neoplasms

We investigated the *in vivo* bone phenotype in T-cell lymphoma with overexpression of PTHrP or MIP-1α. On the day of sacrifice, blood was collected, and plasma calcium was measured. There was no significant difference between plasma calcium concentrations in mice with Jurkat-PTHrP (9.7 mg/dL ± 0.5), Jurkat-MIP-1α (10.1 mg/dL ± 0.1), and Jurkat-pcDNA (9.6 mg/dL ± 1.7) xenografts. The absence of hypercalcemia in the mice with Jurkat-PTHrP xenografts is consistent with local activation of osteoclasts resulting in focal bone resorption, rather than diffuse, whole body bone loss.

Tibial radiographs of the Jurkat-PTHrP mice demonstrated a dramatic increase in radiolucency that ranged from large focal to variably sized multifocal, coalescing areas of bone loss spanning from the proximal metaphysis throughout the diaphysis (Figure 3A). Jurkat-MIP-1α-bearing tibias had evidence of mild to moderate tumor-associated bone loss, characterized by focal to coalescing areas of radiolucency that largely remained confined to the area of the metaphysis and proximal diaphysis (Figure 3B). The tumor-bearing tibias of the Jurkat-pcDNA cell line had minimal evidence of osteolysis (Figure 3C). The percent tumor-associated bone loss was significantly greater in the Jurkat-PTHrP tumor bearing tibias when compared to the tibias of mice bearing Jurkat-MIP-1α or Jurkat-pcDNA neoplasms (Figure 3D). The bioluminescent data (Figure 2) showed that the overall tumor burden was lower in the Jurkat-PTHrP bone neoplasms compared to Jurkat-pcDNA neoplasms, indicating that the increased osteolysis was not a result of greater tumor mass in the tibias.

Jurkat-PTHrP neoplasms had pathologic bone resorption with increased osteoclast number and activity and decreased trabecular bone

H&E-stained tibias from the Jurkat-PTHrP mice revealed sheets of large, round, atypical lymphoma cells with prominent mitoses. Lymphoma cells extended from the proximal metaphysis to the mid- or distal diaphysis. A decrease in the number of trabeculae and total area of trabecular bone was observed, and trabeculae were lined by large, bone-resorbing osteoclasts and eroded surfaces (Figure 4). Activated osteoclasts contained one to multiple round nuclei, and moderate amounts of amphophilic cytoplasm. There were occasional areas of activated osteoclasts adjacent to Jurkat-PTHrP tumor cells that were eroding through the cortex of the bone. Tibias of Jurkat-MIP-1α and Jurkat-pcDNA mice revealed similar lymphoma cells as seen in the Jurkat-PTHrP tumors with cells extending from the

metaphyseal region to varying depths of the tibial diaphysis. In contrast to the Jurkat-PTHrP bone neoplasms, both Jurkat-MIP-1α and Jurkat-pcDNA mice had significantly more trabeculae and endosteal new bone formation (Figure 4B;4C). H&E-stained tibias were scanned and analyzed using Bioquant software to evaluate the amount of trabecular bone. Jurkat-PTHrP bone neoplasms had a significant decrease in the number and area of trabeculae compared to Jurkat-pcDNA and Jurkat-MIP-1α bone neoplasms (Figure 4E).

TRAP-stained tibias from the Jurkat-PTHrP neoplasms had a marked increase in TRAP-positive osteoclasts lining the resorbing surfaces of trabecular and cortical bone (Figure 4D). Osteoclasts were also detached from bone surfaces and found within the medullary cavity associated with tumor cells and admixed with fibrous stroma. TRAP-stained tibias of Jurkat-MIP-1α mice had a mild increase of TRAP-stained osteoclasts that lined the new medullary bone and the growth plate. Bone histomorphometry of TRAP-stained tibias showed a significant increase in the number of TRAP-stained osteoclasts per trabecular surface in the Jurkat-PTHrP bone neoplasms compared to the Jurkat-MIP-1α and Jurkat-pcDNA tibial neoplasms (Figure 4D).

PTHrP did not increase skeletal metastasis in T-cell lymphoma

The bone phenotype in Jurkat-PTHrP xenografts raised the possibility that Jurkat-PTHrP neoplasms may have a tropism for the bone microenvironment. PTHrP overexpression could mediate communication between the lymphoma cells and bone cells to create a pro-tumorigenic microenvironment and promote distant bone metastasis. We tested whether PTHrP would enhance bone metastasis following intracardiac injection. Our hypothesis was that PTHrP is sufficient to increase skeletal metastasis in Jurkat lymphoma cells.

Jurkat-PTHrP and Jurkat-pcDNA cells were injected into the left cardiac ventricle of NSG mice, and *in vivo* bioluminescent imaging was performed weekly to monitor for metastasis. After 24 days, bioluminescent signal was detected in all mice and signal intensity was monitored until the end of the study (Table 1). Six weeks following injection, mice were euthanized and bioluminescent signal was present in the bones of most mice in the two groups. Bioluminescent signal was used to quantify bone metastases between the two groups and showed an increased number of metastatic sites in Jurkat-pcDNA mice compared to Jurkat-PTHrP mice (Fig. 5C and Table 1).

To evaluate potential tumor-induced bone changes, tibias were isolated on the day of sacrifice and high resolution Faxitron imaging and histopathology were performed. There was no evidence of radiographic bone changes in the Jurkat-PTHrP and Jurkat-pcDNA mice that had confirmed tibial bone neoplasms by histopathology, likely due to the small size of the micrometastases. On histopathologic examination, tibias and femurs of Jurkat-PTHrP xenografts showed multifocal to focal areas of lymphoma cells in the diaphysis and were admixed within the hematopoietic population in the marrow (Figure 5A). Bone surfaces that were adjacent to and lined by intramedullary tumor cells showed evidence of cortical erosion. Jurkat-pcDNA xenografts showed multifocal to diffuse distribution of lymphoma cells throughout the diaphysis of the tibia and femur that was frequently seen with extensive necrosis and hemorrhage (Figure 5B). These data demonstrate that, contrary to our hypothesis, PTHrP overexpression does not increase metastasis in Jurkat lymphoma.

Discussion

We developed and characterized a mouse model of human leukemia that can be used to investigate the mechanisms and tumor-bone signaling factors responsible for the bone phenotypes T-cell leukemia. When the Jurkat T-cell line was injected into the marrow cavity of NSG mice, the tumor cells proliferated within the marrow inducing minimal bone cell response. Previous reports have demonstrated that several factors secreted from HTLV-1-infected cells can induce *ex vivo* bone resorption and osteoclast activity, including PTHrP and MIP-1α. Therefore, we evaluated the individual contribution of PTHrP and MIP-1α to the osteolytic tumor-bone phenotype using overexpression technology and intratibial xenograft models.

PTHrP expression has been identified in multiple types of cancer including breast cancer, prostate cancer, ATL, multiple myeloma, and several other malignancies [12]. PTHrP can function as an endocrine, paracrine, autocrine, and/or intracrine hormone depending on the tumor type [26]. HHM occurs in 80% of ATL patients [27,28]. Constitutive expression of PTHrP by lymphoma cells was reported in ATL patients, resulting in whole-body osteoclast activation and bone resorption and increased renal tubule reabsorption of calcium [29]. When human peripheral blood mononuclear cells were transformed in vitro by the HTLV-1 virus, both PTHrP and the PTH1 receptor were upregulated, suggesting a potential autocrine role for PTHrP in ATL [9]. Osteolytic bone metastases frequently occur in breast cancer patients with advanced disease with greater than 90% of bone metastatic sites expressing PTHrP [30]. Overexpression and knockdown of PTHrP in breast cancer has identified a role for PTHrP in enhancing breast cancer-mediated osteolysis and induction of cancer-associated hypercalcemia [31–33]. PTHrP can decrease bone metastases if it is expressed in primary breast tumors [34]. In prostate cancer, bone metastases with PTHrP expression are often osteoblastic, and are characterized by pathologic new bone formation [11].

In this study, we found that PTHrP expression by the Jurkat T-lymphocyte resulted in paracrine-mediated osteolysis and was sufficient to recapitulate the osteolytic lesions seen in ATL bone tumors, demonstrating a significant paracrine role for PTHrP in osteolytic lymphoma lesions. Although overexpression of PTHrP was sufficient to induce marked pathologic osteolysis, PTHrP overexpression also modified other bone signaling genes in the Jurkat cells [24], suggesting a potential synergistic, or cooperative role for PTHrP in osteolysis.

MIP-1α has been shown to have an important role in HHM and in promoting tumor growth and metastasis in ATL and other osteolytic bone neoplasms such as multiple myeloma [6,9,10,19,23,35,36]. MIP-1α has been consistently detected in the serum of ATL patients with hypercalcemia. In one study, 24/24 hypercalcemic ATL patients had circulating MIP-1α, whereas it was rarely identified in normocalcemic ATL patients [19]. MIP-1α can induce osteoclast formation and activity through both RANKL-dependent and independent mechanisms [37]. MIP-1α has been shown to significantly enhance human osteoclast precursor migration and RANKL expression by ATL cells [19]. ATL osteolytic primary bone neoplasms were positive for MIP-1α by immunohistochemistry even when they were negative for PTHrP [16]. Despite the evidence to suggest that overexpression of MIP-1α by

Jurkat T cells would cause pathologic osteolysis, we found minimal increases in osteolysis between Jurkat- MIP-1α-luc and Jurkat-pcDNA cells *in vivo*. These results suggest that additional intrinsic factors, or cooperative tumor-associated cytokines are required for MIP-1α-mediated bone resorption and hypercalcemia in ATL and T-cell lymphoma.

PTHrP has been associated with the progression of skeletal metastasis in breast, prostate, and lung cancers [11,38–40]. Breast cancers that overexpress PTHrP can be less invasive/aggressive, but have more bone resorption [34]. The high incidence of PTHrP and bone metastasis seen in ATL patients suggested that PTHrP may have a role in promoting skeletal metastasis in ATL. However, PTHrP overexpression in Jurkat T cells did not increase the incidence of bone metastasis following intracardiac injections when compared to controls. Our findings were consistent with the idea that PTHrP overexpression does not increase skeletal metastasis in T cell lymphoma and suggests that other factors are responsible for the multifocal bone involvement of human patients.

In conclusion, we investigated the potential of two factors that are highly expressed in ATL using a mouse model of T-cell lymphoma in bone. Our studies show that PTHrP overexpression resulted in paracrine-mediated osteolytic bone resorption characterized by increased osteoclast number and decreased trabecular bone *in vivo*, and increased calvarial bone loss *ex vivo*. These results demonstrate an important role of PTHrP in pathologic bone loss in T-cell lymphoma. We found that PTHrP did not increase the incidence of skeletal metastasis, suggesting that other factors are responsible for bone involvement in T-cell lymphoma. We showed that MIP-1α overexpression alone did not significantly increase local osteolysis in T-cell lymphoma. Our development of this novel mouse model of lymphoma in bone will be useful for future investigations of the independent and synergistic functions of individual factors that potentially play a role in the leukemia-bone communication and could be useful therapeutic targets in the future.

Acknowledgments

This work was funded through grants from the National Cancer Institute (P01 CA100730 to TJR and KNW) and (T32 OD010429 to NAK). Animal research reported in this publication was supported by the Ohio State University Comprehensive Cancer Center and the National Institutes of Health under grant number P30 CA016058. We thank the Target Validation Shared Resource (TVSR) at the Ohio State University Comprehensive Cancer Center for providing the NSG mice used in the preclinical studies described herein. The content is solely the responsibility of the authors and does not necessarily represent the official views of the National Institute of Health. We thank Alan Flechtner and Anne Saulsbery for tissue processing and preparation of slides. Finally, we thank our medical illustrator Tim Vojt for his invaluable assistance in creating all the figures.

References

1. Graham RL, Burch M, Krause JR. Adult T-cell leukemia/lymphoma. Proc (Bayl Univ Med Cent) 2014;27:235–238. [PubMed: 24982574]
2. Matutes E Adult T-cell leukaemia/lymphoma. J Clin Pathol 2007;60:1373–1377. [PubMed: 18042693]
3. Shu ST, Martin CK, Thudi NK, Dirksen WP, Rosol TJ. Osteolytic bone resorption in adult T-cell leukemia/lymphoma. Leuk Lymphoma 2010;51:702–714. [PubMed: 20214446]
4. Honda S, Yamaguchi K, Miyake Y, et al. . Production of parathyroid hormone-related protein in adult T-cell leukemia cells. Jpn J Cancer Res 1988;79:1264–1268. [PubMed: 3148595]

5. Motokura T, Fukumoto S, Matsumoto T, et al. . Parathyroid hormone-related protein in adult T-cell leukemia-lymphoma. Ann Intern Med 1989;111:484–488. [PubMed: 2549824]
6. Prager D, Rosenblatt JD, Ejima E. Hypercalcemia, parathyroid hormone-related protein expression and human T-cell leukemia virus infection. Leuk Lymphoma 1994;14:395–400. [PubMed: 7812198]
7. Watanabe T, Yamaguchi K, Takatsuki K, Osame M, Yoshida M. Constitutive expression of parathyroid hormone-related protein gene in human T cell leukemia virus type 1 (HTLV-1) carriers and adult T cell leukemia patients that can be trans-activated by HTLV-1 tax gene. J Exp Med 1990;172:759–765. [PubMed: 2388034]
8. Yamaguchi K, Kiyokawa T, Watanabe T, et al. . Increased serum levels of C-terminal parathyroid hormone-related protein in different diseases associated with HTLV-1 infection. Leukemia 1994;8:1708–1711. [PubMed: 7934167]
9. Nadella MV, Shu ST, Dirksen WP, et al. . Expression of parathyroid hormone-related protein during immortalization of human peripheral blood mononuclear cells by HTLV-1: implications for transformation. Retrovirology 2008;5:46. [PubMed: 18541021]
10. Richard V, Lairmore MD, Green PL, et al. . Humoral hypercalcemia of malignancy: severe combined immunodeficient/beige mouse model of adult T-cell lymphoma independent of human T-cell lymphotropic virus type-1 tax expression. Am J Pathol 2001;158:2219–2228. [PubMed: 11395400]
11. Liao J, Li X, Koh AJ, et al. . Tumor expressed PTHrP facilitates prostate cancer-induced osteoblastic lesions. Int J Cancer 2008;123:2267–2278. [PubMed: 18729185]
12. Liao J, McCauley LK. Skeletal metastasis: Established and emerging roles of parathyroid hormone related protein (PTHrP). Cancer Metastasis Rev 2006;25:559–571. [PubMed: 17165129]
13. Soki FN, Park SI, McCauley LK. The multifaceted actions of PTHrP in skeletal metastasis. Future Oncol 2012;8:803–817. [PubMed: 22830401]
14. Takayama Y, Mori T, Nomura T, Shibahara T, Sakamoto M. Parathyroid-related protein plays a critical role in bone invasion by oral squamous cell carcinoma. Int J Oncol 2010;36:1387–1394. [PubMed: 20428761]
15. Fiaschi-Taesch NM, Stewart AF. Minireview: parathyroid hormone-related protein as an intracrine factor--trafficking mechanisms and functional consequences. Endocrinology 2003;144:407–411. [PubMed: 12538599]
16. Hara T, Wakatsuki S, Ozaki S, Abe M, Kosaka M. Primary adult T-cell leukemia/lymphoma of bone. Int J Hematol 2004;79:157–160. [PubMed: 15005344]
17. Kuriyama T, Kawano N, Yamashita K, Kikuchi I. Two cases of primary adult T-cell leukemia/lymphoma of bone: case reports and a review of the literature. Int J Hematol 2016.
18. Chiba K, Hashino S, Izumiyama K, et al. . Multiple osteolytic bone lesions with high serum levels of interleukin-6 and CCL chemokines in a patient with adult T cell leukemia. Int J Lab Hematol 2009;31:368–371. [PubMed: 18177436]
19. Okada Y, Tsukada J, Nakano K, Tonai S, Mine S, Tanaka Y. Macrophage inflammatory protein-1alpha induces hypercalcemia in adult T-cell leukemia. J Bone Miner Res 2004;19:1105–1111. [PubMed: 15176993]
20. Tanaka Y, Mine S, Figdor CG, et al. . Constitutive chemokine production results in activation of leukocyte function-associated antigen-1 on adult T-cell leukemia cells. Blood 1998;91:3909–3919. [PubMed: 9573029]
21. Kukita T, Nomiyama H, Ohmoto Y, et al. . Macrophage inflammatory protein-1 alpha (LD78) expressed in human bone marrow: its role in regulation of hematopoiesis and osteoclast recruitment. Lab Invest 1997;76:399–406. [PubMed: 9121122]
22. Scheven BA, Milne JS, Hunter I, Robins SP. Macrophage-inflammatory protein-1alpha regulates preosteoclast differentiation in vitro. Biochem Biophys Res Commun 1999;254:773–778. [PubMed: 9920817]
23. Hata H Bone lesions and macrophage inflammatory protein-1 alpha (MIP-1a) in human multiple myeloma. Leuk Lymphoma 2005;46:967–972. [PubMed: 16019547]
24. Shu ST, Dirksen WP, Lanigan LG, et al. . Effects of parathyroid hormone-related protein and macrophage inflammatory protein-1alpha in Jurkat T-cells on tumor formation in vivo and

expression of apoptosis regulatory genes in vitro. Leuk Lymphoma 2012;53:688–698. [PubMed: 21942940]

25. Simmons JK, Dirksen WP, Hildreth BE 3rd, et al. . Canine prostate cancer cell line (Probasco) produces osteoblastic metastases in vivo. Prostate 2014;74:1251–1265. [PubMed: 25043424]
26. McCauley LK, Martin TJ. Twenty-five years of PTHrP progress: from cancer hormone to multifunctional cytokine. J Bone Miner Res 2012;27:1231–1239. [PubMed: 22549910]
27. Clines GA. Mechanisms and treatment of hypercalcemia of malignancy. Curr Opin Endocrinol Diabetes Obes 2011;18:339–346. [PubMed: 21897221]
28. Shu S Pathogenesis and Treatments of Humoral Hypercalcemia of Malignancy in Adult T-Cell Leukemia/Lymphoma Induced by Human T Lymphotropic Virus Type 1 2009.
29. Takaori-Kondo A, Imada K, Yamamoto I, et al. . Parathyroid hormone-related protein-induced hypercalcemia in SCID mice engrafted with adult T-cell leukemia cells. Blood 1998;91:4747–4751. [PubMed: 9616173]
30. Powell GJ, Southby J, Danks JA, et al. . Localization of parathyroid hormone-related protein in breast cancer metastases: increased incidence in bone compared with other sites. Cancer Res 1991;51:3059–3061. [PubMed: 2032246]
31. Guise TA, Yin JJ, Taylor SD, et al. . Evidence for a causal role of parathyroid hormone-related protein in the pathogenesis of human breast cancer-mediated osteolysis. J Clin Invest 1996;98:1544–1549. [PubMed: 8833902]
32. Guise TA, Yin JJ, Thomas RJ, Dallas M, Cui Y, Gillespie MT. Parathyroid hormone-related protein (PTHrP)-(1–139) isoform is efficiently secreted in vitro and enhances breast cancer metastasis to bone in vivo. Bone 2002;30:670–676. [PubMed: 11996903]
33. Wysolmerski JJ, Dann PR, Zelazny E, et al. . Overexpression of parathyroid hormone-related protein causes hypercalcemia but not bone metastases in a murine model of mammary tumorigenesis. J Bone Miner Res 2002;17:1164–1170. [PubMed: 12096830]
34. Henderson MA, Danks JA, Slavin JL, et al. . Parathyroid hormone-related protein localization in breast cancers predict improved prognosis. Cancer Res 2006;66:2250–2256. [PubMed: 16489028]
35. Shu ST, Nadella MV, Dirksen WP, et al. . A novel bioluminescent mouse model and effective therapy for adult T-cell leukemia/lymphoma. Cancer Res 2007;67:11859–11866. [PubMed: 18089816]
36. Oyajobi BO, Franchin G, Williams PJ, et al. . Dual effects of macrophage inflammatory protein-1alpha on osteolysis and tumor burden in the murine 5TGM1 model of myeloma bone disease. Blood 2003;102:311–319. [PubMed: 12649140]
37. Oba Y, Lee JW, Ehrlich LA, et al. . MIP-1alpha utilizes both CCR1 and CCR5 to induce osteoclast formation and increase adhesion of myeloma cells to marrow stromal cells. Exp Hematol 2005;33:272–278. [PubMed: 15730850]
38. Li J, Karaplis AC, Huang DC, et al. . PTHrP drives breast tumor initiation, progression, and metastasis in mice and is a potential therapy target. J Clin Invest 2011;121:4655–4669. [PubMed: 22056386]
39. Linforth R, Anderson N, Hoey R, et al. . Coexpression of parathyroid hormone related protein and its receptor in early breast cancer predicts poor patient survival. Clin Cancer Res 2002;8:3172–3177. [PubMed: 12374685]
40. Pecherstorfer M, Schilling T, Blind E, et al. . Parathyroid hormone-related protein and life expectancy in hypercalcemic cancer patients. J Clin Endocrinol Metab 1994;78:1268–1270. [PubMed: 8175989]

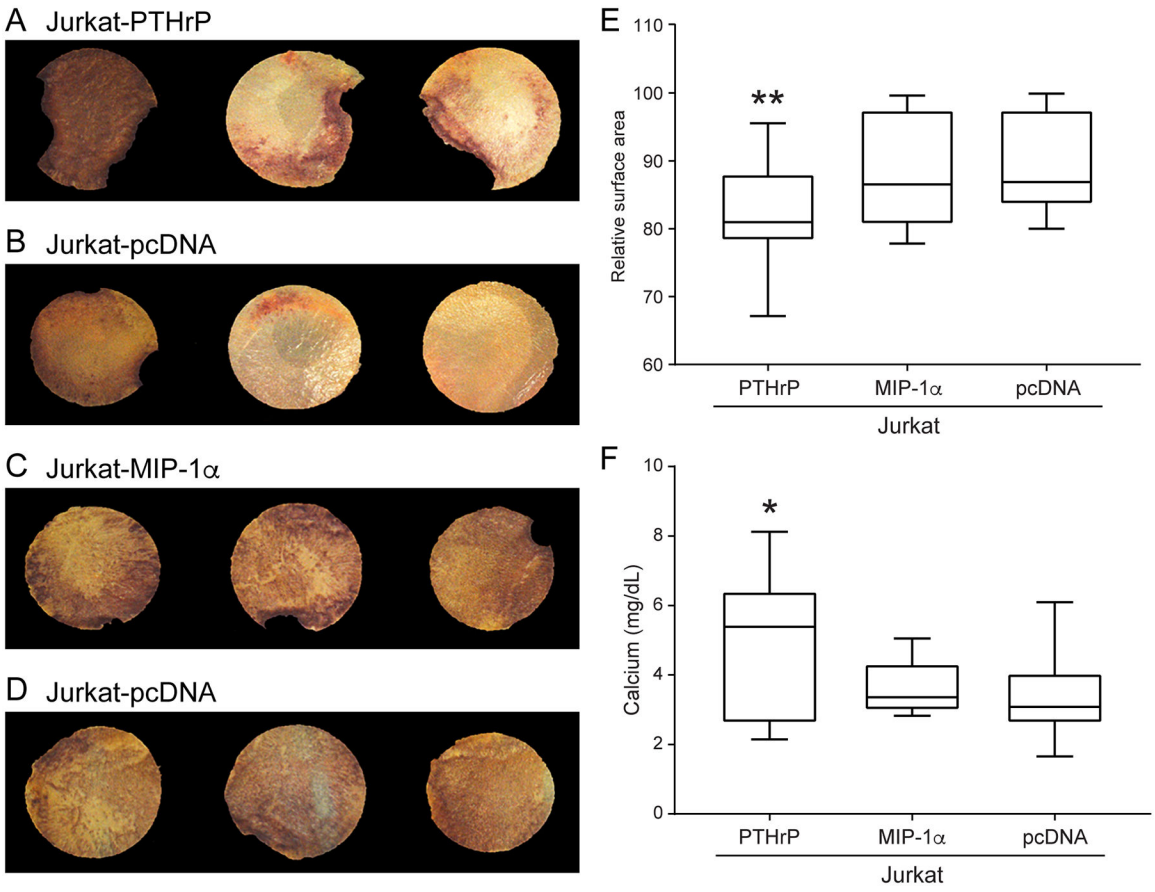

Figure 1.

Conditioned medium from Jurkat-PTHrP cells had greater bone resorption and calcium release in ex vivo experiments. (A–D) Neonatal calvarial discs co-cultured with conditioned media from Jurkat cells and TRAP-stained for osteoclast activity. Vertical pairs were from the same mouse, thus each PTHrP-pcDNA and MIP-1-pcDNA comparison was internally controlled. (E) Jurkat-PTHrP conditioned medium significantly decreased bone area of calvaria due to increased osteoclastic bone resorption comparedto Jurkat-pcDNA as indicated by a decrease in calvarial area (**$p < .01$). (F) Co-cultures resulted in higher concentrationsof calcium in the medium containing the calvaria and conditioned medium from the Jurkat-PTHrP cells when compared to Jurkat-MIP-1α and Jurkat-pcDNA cells (*$p < .03$).

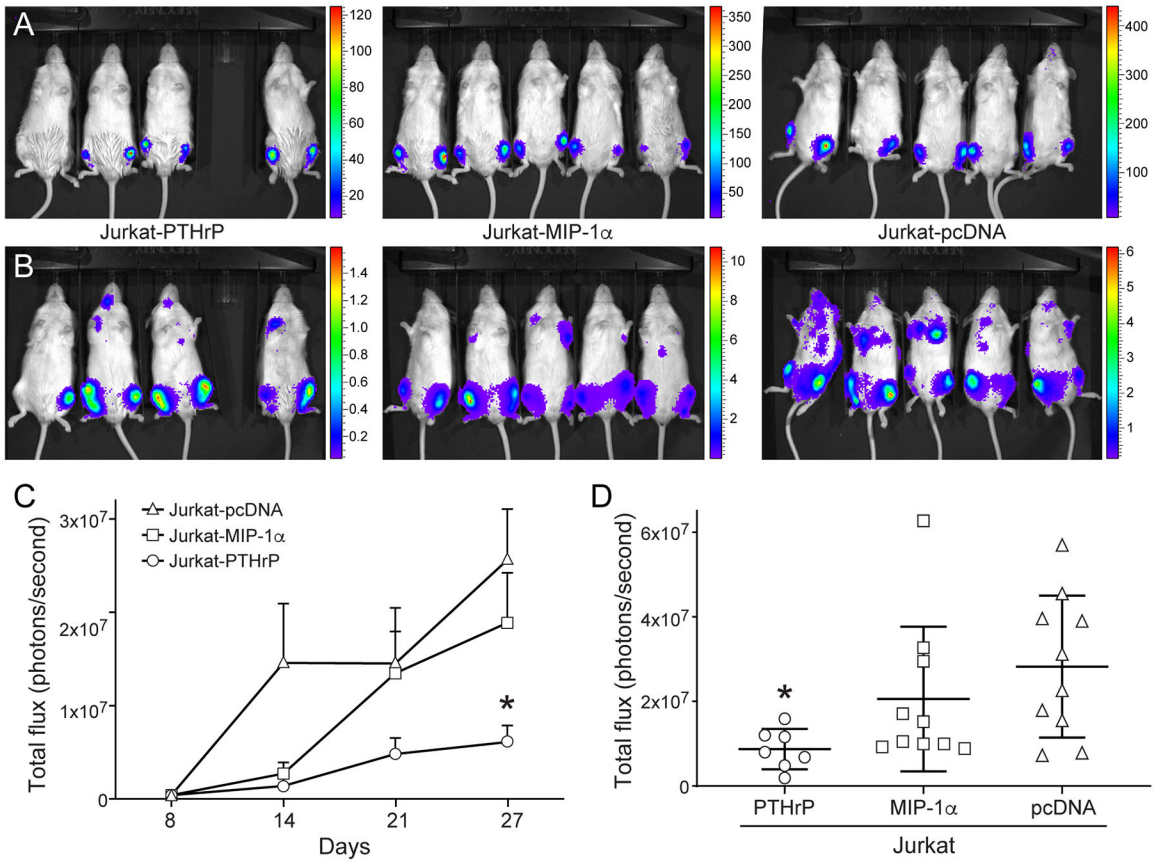

Figure 2.

In vivo bioluminescent imaging showing Jurkat-PTHrP tibial neoplasms grew at a significantly slower rate than JurkatpcDNA neoplasms. Bioluminescent imaging of mice with Jurkat cells with overexpression of PTHrP, MIP-1α, or vector mRNA control. (A) Successful tibial engraftment was confirmed on the first week of bioluminescent imaging. Y-axes are $\times 10^3$. (B) On day 30 (sacrifice) tibial tumor burden had increased in all groups. Y-axes are $\times 10^6$. (C) The Jurkat-pcDNA tibial neoplasms had the greatest bioluminescent signal. Jurkat-pcDNA bone neoplasms grew at a significantly faster rate than Jurkat-PTHrP bone neoplasms (*p <.05). (D) On the day of sacrifice, overall tibial tumor burden was significantly decreased in the Jurkat-PTHrP mice, as determined by decreased intensity of bioluminescence in the tibias (*p < .05).

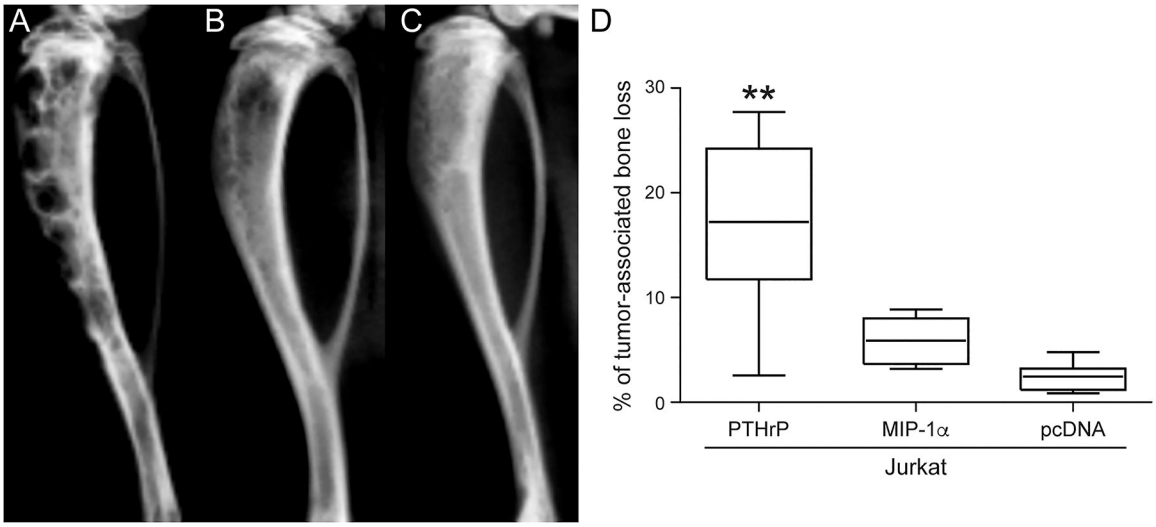

Figure 3.

Radiographic bone loss was significantly greater in the Jurkat-PTHrP tumor-bearing tibias. (A) Tibias with Jurkat-PTHrP neoplasms had significantly greater bone loss as indicated by the total area of radiolucency. Multifocal to coalescing areas of radiolucency spanned from the proximal metaphysis to the mid- to distal diaphysis in Jurkat-PTHrP-bearing bone neoplasms. (B) Jurkat-MIP-1α -bearing tibias had focal to coalescing areas of radiolucency that were significantly less than the Jurkat-PTHrP neoplasms but more than Jurkat-pcDNA tumor-bearing tibias. (C) Jurkat-pcDNA tibial bone neoplasms had minimal areas of radiolucency. (D) Bone loss was quantified on high-resolution faxitron images using Bioquant software. Jurkat-PTHrP mice had significantly greater tumor-associated bone loss than Jurkat-MIP-1α and JurkatpcDNA (**$p < .01$).

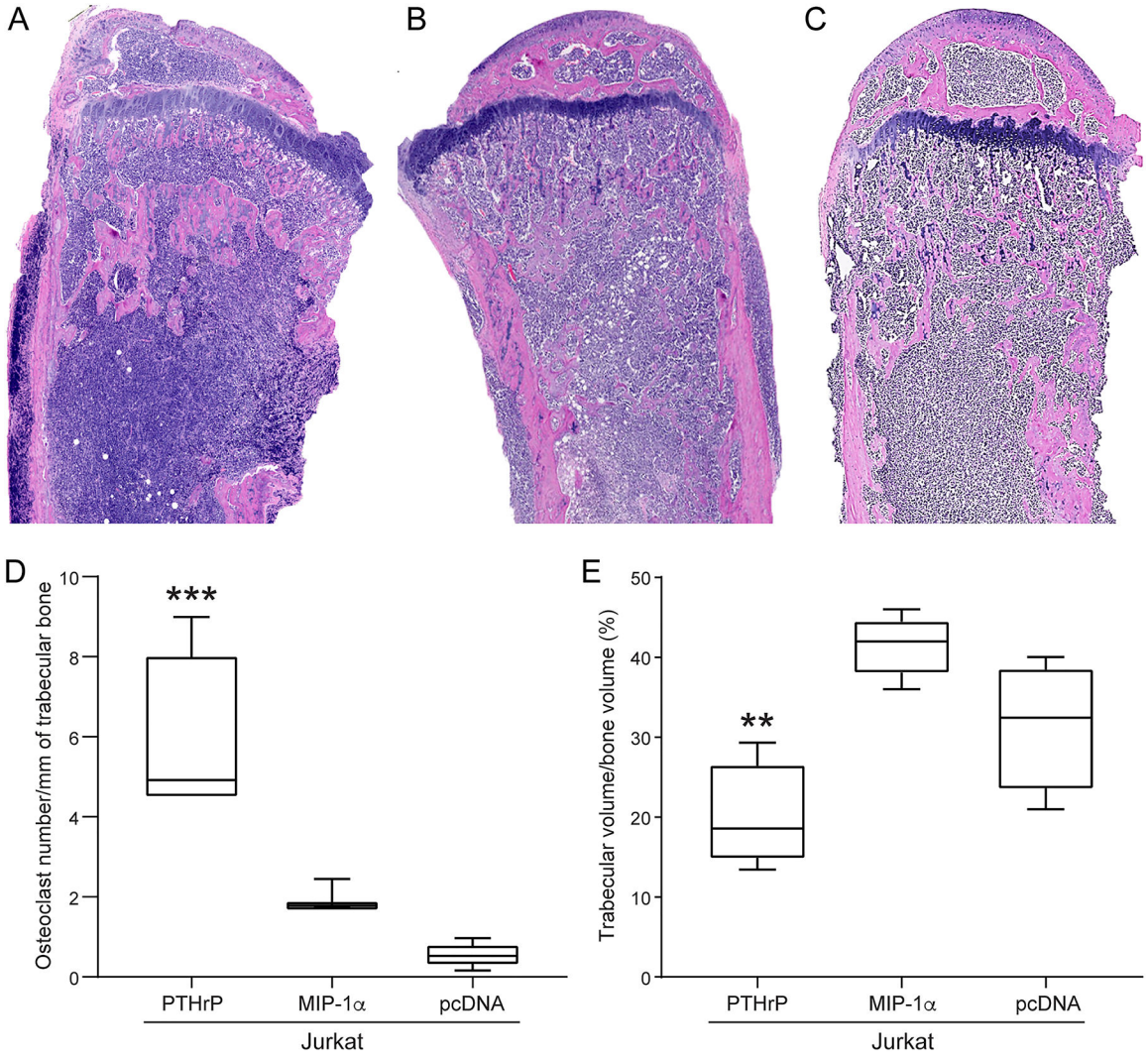

Figure 4.

Jurkat-PTHrP neoplasms had increased osteoclast number and decreased trabecular bone volume. (A) H&E-stained tibias from the Jurkat-PTHrP mice had lymphoma cells that spanned from the proximal metaphysis to the mid- to distal diaphysis. A decrease in the number and total area of trabecular bone was present. Tibias of Jurkat-MIP-1α (B) and Jurkat-pcDNA (C) mice had lymphoma cells spanning from the metaphysis to varying depths of the tibial diaphysis. Endosteal new bone formation was present adjacent to the lymphoma cells within the metaphysis in both Jurkat-MIP-1a and Jurkat-pcDNA mice. (D) The number of osteoclasts per surface of trabecular bone and the number of osteoclasts was significantly increased in Jurkat-PTHrP tumor-bearing tibias when compared with Jurkat-pcDNA and Jurkat-MIP-1α mice (***$p < .001$). (E) The area of trabecular bone was significantly decreased in the Jurkat-PTHrP mice compared to the Jurkat-pcDNA and Jurkat-MIP-1α mice (**$p < .004$).

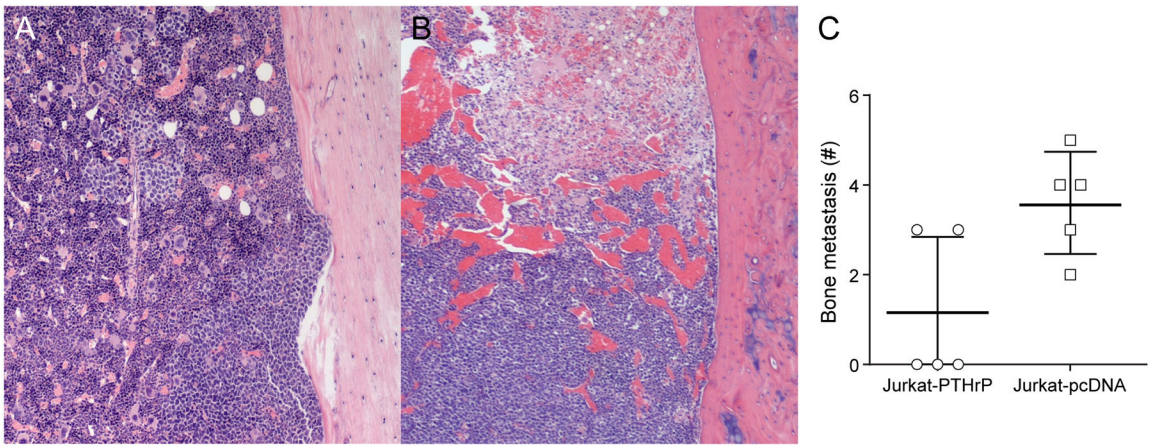

Figure 5.

PTHrP did not increase the incidence of skeletal metastasis following intracardiac injection of Jurkat-PTHrP cells. (A) H&E-stained tibias of Jurkat-PTHrP bone metastases following intracardiac injection. Metastases had a multifocal distribution in the tibias and occasionally lymphoma cells were seen adjacent to eroded cortices (bottom potion of the bone). (B) In contrast, JurkatpcDNA tibial metastases were characterized by a diffuse distribution with extensive necrosis and hemorrhage. Tibial and femoral metastases were confirmed by histopathology. (C) The average incidence of bone metastasis was greater in the Jurkat-pcDNA mice than Jurkat-PTHrP mice, indicating that PTHrP did not increase the incidence of Jurkat cell bone metastases.

Table 1-

Distant metastases for Jurkat-pcDNA and Jurkat-PTHrP were evaluated by bioluminescent imaging and histopathology.

Cell line	Mouse number	Metastasis				
		Tibia	Tibia	Femur	Histopathologic metastasis	BLI metastasis
Jurkat-pcDNA	M1	X	X	X	-	-
Jurkat-pcDNA	M2	X	X	X	Vertebrae, humerus	Stomach, vertebrae, humerus
Jurkat-pcDNA	M3	X	X	-	Vertebrae	Vertebrae
Jurkat-pcDNA	M4	X	X	-	-	-
Jurkat-pcDNA	M5	X	X	X	Vertebrae	Vertebrae
Jurkat-PTHrP	M6	X	X	X	Extranodal (fat)	Stomach, extranodal (fat)
Jurkat-PTHrP	M7	X	X	X	-	-
Jurkat-PTHrP	M8	-	-	-	-	-
Jurkat-PTHrP	M9	-	-	-	-	Stomach
Jurkat-PTHrP	M10	-	-	-	-	-